This article has been accepted for publication in a future issue of this journal, but has not been fully edited. Content may change prior to final publication. Citation information: DOI 10.1109/OJAP.2021.3081992, IEEE Open Journal of Antennas and Propagation

Dielectric Rod Antenna Array With Planar Folded Slot Antenna Excitation

Gabriel L. Saffold, *Member, IEEE* and Thomas M. Weller *Fellow, IEEE*

A dielectric rod antenna array fed by slot antenna radiators without the use of metallic waveguide is presented here. Communication systems, especially those related to 5G, are moving up into mm-wave bands where metal losses can become significant and many traditional fabrication and manufacturing techniques become more difficult. Dielectric rod antennas (DRA) are entirely made of dielectric and may be injection-molded or 3D-printed as solid rods, layered rods, or tubes. While the normal approach to feeding DRAs involves some version of metallic waveguide, we show here that the DRA may be integrated with a planar radiator feed and used effectively in an array configuration. The array demonstrated is a 2 x 2 array designed for operation at 15 GHz. Each DRA is 6λ long. The array is fabricated on a 100 mm x 100 mm substrate with 52 mm separation between elements. The array radiation efficiency is 80% for an array gain of 19 dBi.

***Index Terms*—Dielectric Rod Antennas, Ku-band, 3D Printing**

I. INTRODUCTION

THIS paper presents the design and performance of a 2 x 2 array of 3D printed cylindrical high gain dielectric rod antennas that is integrated with a planar feed network. Unlike existing DRA array designs, this array does not use metallic waveguide as part of the feed mechanism or support for each dielectric rod. Given the relative simplicity of feeding the array of high gain antennas using planar transmission lines, the technology is amenable to low cost, compact package-level integration. These could be useful for mm-wave base-stations, automotive radar, directional wireless routers and similar applications.

As communication technologies continue to move toward operation at higher frequencies, especially with the current push into mm-wave bands, dielectric rod antennas (DRA) are a good low-cost alternative for achieving high gain with minimal use of metal. Dielectric structures do not suffer from the losses associated with metallic structures of similar size. Dielectric rods, used in conjunction with an underlying radiating feed, increase the overall gain of the feed radiator and offer more flexibility in manufacturing. Direct integration of dielectric rods onto planar circuit radiators is demonstrated here with inexpensive, 3D printed ABS dielectric rods. Although these rods are not directly printed on the RF circuits in this work, the principle is validated.

DRAs have been used in radar antenna arrays [1] - [3], millimeter-wave imaging [4], and other applications [5], [6]. The feed mechanisms for the dielectric rods typically include some form of a metallic waveguide for support or for setting up the modes necessary for launching a surface wave along the rod. Most of these are hollow metallic waveguide-fed designs [4], [7]–[17]. In other designs, the metallic waveguide is used in conjunction with a planar radiator, as in [18]–[21]. Chu and Kilcoyne [22] feed a DRA with a helix. Abumunshar and Sertel [23] as well as Liu and Chen [24] use a unique v-shaped two-wire TEM waveguide feed along a feed taper in the DRA. A DRA to DRA, on-chip communication system uses dielectric rod waveguide-fed DRAs [25]. Other planar-integrated DRAs have been fed without hollow metallic waveguides including those fed with an edge-fed design using antipodal Vivaldi antennas [5], a stacked patch [6], and direct contact between the DRA and a ring-slot [26]. Rivera-Lavado et al. [27], [28] demonstrate THz DRAs fed by integration of the dielectric rod with a planar, linearly polarized log-periodic radiator.

Several of the works referenced above include arrays: both with non-planar feeds [2], [4], [9], [14], [17] and planar-integrated feeds [18], [21]. While there are planar-fed DRAs without metallic waveguides, as mentioned above, there are no instances known to the authors of planar-integrated arrays of DRAs which do not use hollow metallic waveguides as part of the feed structure. This work fills that gap.

The metallic waveguide is advantageous for physical stability and for a more efficient launch of the surface wave along the rod. At lower frequencies, where metallic losses are insignificant and metal is easily formed, the use of a metallic waveguide with a planar feed may be preferable. However, the metallic waveguide is not necessary for a single DRA or for an array of planar-fed DRAs, as demonstrated here. Using a feed without a metallic waveguide is a useful option for additive manufacturing. It makes it possible to fabricate a planar circuit using traditional, cost-effective techniques and then to integrate the planar circuit with 3d printed, non-metallic radiators. The unique benefit of the array design presented here is its ease of fabrication combined with a limited use of metal in the combination of the feed and radiator.

This paper reviews the theory of operation of DRAs, followed by a detailed presentation of the design of a four-element, 2 x 2, folded dipole slot-fed DRA array. Sections III through V examine different aspects of individual planar-fed DRA design. The planar-fed DRAs are designed using a novel procedure based on design guidelines for surface wave antennas [29]. A modification to the surface wave antenna

Manuscript received March 30, 2021.

G. L. Saffold is with the Georgia Tech Research Institute, Atlanta, GA 30080 USA (corresponding author phone: 404-407-6325; e-mail: gabriel.saffold@gtri.gatech.edu)."

T. M. Weller is with the School of Electrical Engineering and Computer Science, Oregon State University, Corvallis, OR 97331 USA (e-mail: tom.weller@oregonstate.edu).

design procedure is made for improved prediction of planar-fed DRA gain. The planar-fed DRA has a gain of $16.5\ dBi$ with a radiation efficiency of 96%. Section VI expands on the individual planar-fed design to a 2 x 2 array of planar-fed DRAs along with comparison of associated simulations and measurements. The array radiation efficiency is 80% at 15 GHz for an array gain of 19 dBi. All simulations in this paper were performed using the Ansys High Frequency Structure Simulator (HFSS) version 2020R1.

II. Dielectric Rod Antenna Theory of Operation

The dielectric rod antenna is best understood as a special case of a dielectric rod waveguide. As with all waveguides, the chief performance objective is to convey the energy in some mode from an input feed point to an output point with minimal loss. Kiely [30] credits work by Hondros and Debye [31] as the earliest theoretical treatment of the use of a solid dielectric cylinder to convey electromagnetic energy from one port to another with low loss.

Early experimental work with dielectric cylinders as waveguides revealed their tendency to radiate at bends and discontinuities. Kiely credits unpublished work by Mallach as referenced by Zinke as the first effort to exploit the tendency to radiate at discontinuities by exciting a dielectric cylinder at one end and examining the radiation from the discontinuity at the other end. This configuration resulted in a single lobed end-fire radiation pattern in the direction of the cylinder axis with a proportional relationship between the length of the rod and the directivity of the radiation pattern. Several theories have been proposed to explain the radiation characteristics from a dielectric rod, including the mechanism of radiation and its relationship with rod material characteristics and dimensions for both uniform and tapered rods.

The radiation characteristics of dielectric rod antennas have been explained using variations on Huyghens principle and ray tracing methods [2], [32], by analogy to a dielectric lens [33], by calculation of fictitious surface currents along the surface of the rod using the Schelkunoff Equivalence Principle [30], [34], leaky-wave theory [35], [36], and by the discontinuity radiation concept [29], [37]–[39]. The discontinuity radiation concept is used in Zucker's design method for DRAs [29]. The analysis here is based on Zucker's method.

Huyghens principle with ray tracing theory uses constant phase wave fronts represented by vectors either reflecting or refracting at the outer interface of the rod, at the step discontinuity between inner and outer dielectric constants [2], [32]. Reflected waves continue to travel along the rod while refracted waves radiate from the surface of the rod and contribute to the far-field pattern. Wilkes' degenerate dielectric lens approach is similar [33]. These theories match well with experimental results in the main beam, but do not match well outside the first null beamwidth [30].

Watson and Horton use the Schelkunoff Equivalence Principle to explain dielectric rod radiation from a metallic waveguide-fed, rectangular cross-section dielectric rod. One iteration [34] begins with the assumption that radiation from a dielectric rod results from a standing wave along the rod. A second iteration [40] of their analysis assumes a travelling wave along the rod. An exact representation of the fields and currents on the surface of a rectangular cross-section rod is difficult. Horton [41] also examined uniform rods of circular cross section. In each case, they calculate radiation patterns on the basis of electromagnetic fields produced from fictitious electric and magnetic surface currents along uniform dielectric rods. In the first two cases, they determine the results have good agreement with experiment for uniform rods between 3λ and 6λ long and significant disagreement with experiment beyond 6λ. Horton's application of this theory to a cylindrical rod [41], as with the other two cases, ignores radiation from the ends of the rod. Unlike the other two cases, the case of the cylindrical rod does not agree well with experiment without a correction factor applied to reduce the diameter used in calculation from the actual diameter of the rod. This adjustment dramatically improves agreement.

Since characterizations of dielectric rod waveguides have shown them to have very low loss along the length of the rod [42], [43], James [38] modified Horton's cylindrical rod calculations by including the ends of the rod in the calculations and assuming no radiation along the length of the rod. This rearrangement agrees well with Horton's published empirical data, without the need for the adjustment factor applied to the diameter of the rod. In general, for uniform cross-section rods, methods which negate or minimize the contribution of radiation from the feed and termination ends of the rod are the least accurate when compared to experimental results.

Brown and Spector [37] proposed a theory based on the idea that radiation does not occur along the length of a uniform rod, leaving radiation to occur only at discontinuities. For a uniform rod, the discontinuities are at the feed and terminal points. At the terminal point, the surface wave fields, which necessarily extend outward beyond the surface of the rod, form an aperture much like the aperture at the opening of a metallic horn antenna. This terminal aperture is larger than the cross-sectional area of the rod and can be used to calculate the fields of the radiation pattern. However, accounting for radiation only from the end of the rod does not produce good agreement with radiation measurements, nor does it account for the major discontinuity at the rod feed. When the total fields at the terminal aperture include both those resulting from the surface wave and also those resulting from the radiation at the feed, the agreement between theory and experiment improves. In particular, the addition of contributions to the fields at the terminal aperture from the fields at the feed creates a better predictor of the location of the first nulls and, consequently, the DRA's beamwidth and gain. James [38] notes an error in Brown and Spector's calculations. Correcting the error results in better agreement between the calculation and experimental results. The method has been reviewed [39] and experimentally verified [44]. It is also the basis for modern surface wave antenna design [29].

The method applies also to rods with successive discontinuities. Rather than a continuous taper, Simon and Weill [45] use conducting disks of decreasing diameter, which act as successive discontinuities creating radiating fields that contribute to the fields at the terminal aperture, thereby affecting the

overall radiation pattern. Radiation from smooth, continuous tapers, on the other hand, behave according to the leaky wave antenna theories discussed by Watson [34] as validated by Brown and Spector [37] and James [38], since continuous tapers are continuous discontinuities.

Brown and Spector [37] also established a link between half power beamwidth and relative phase velocity as expressed in terms of the ratio of wavelengths outside and inside the rod, which is also the ratio between the inner and outer wave velocities. This is an important relationship, along with the link between cross-sectional dimension and relative phase velocity, which forms the foundation of DRA design and the ability to dictate DRA performance through careful design of the rod's physical dimensions.

Studies of attenuation along dielectric rods led to expressions of the relative phase velocities between a wave outside and inside the rod as a function of cross-sectional rod dimensions [30], [42], [43]. Similar studies carried out by Astrahan [46] and Jakes [47] explored attenuation along a dielectric tube and found a connection between the two, revealing the dielectric rod as a special case of a dielectric tube, wherein a rod is a tube in which the radius of the innermost, lower dielectric constant cylinder is reduced to zero leaving the higher dielectric outer shell of the tube as the material of the solid rod. The results for attenuation along the rod yield expressions for the relationship between phase velocities along the rod and the cross-sectional dimensions of the rod. These relationships facilitate control over the phase velocity through specification of cross-sectional dimensions, as in Figure 1 for different values of DRA permittivity ϵ_r. The curves in Fig. 1 are calculated using numerical methods to solve for the attenuation along the rod as in [43].

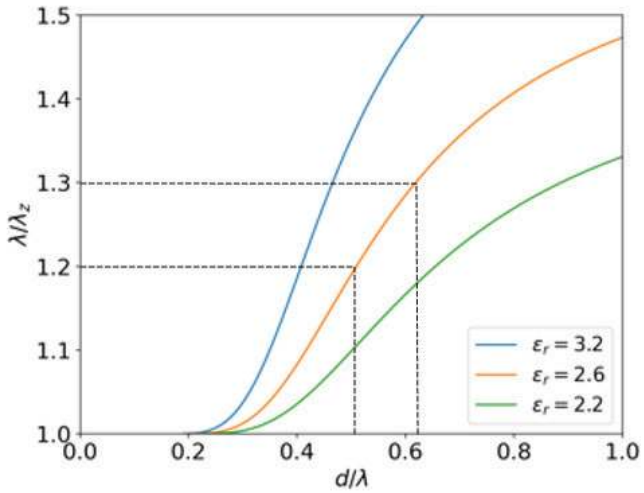

Fig. 1: Design curves for cylindrical DRAs at 15 GHz relating the relative wavelength, $\frac{\lambda}{\lambda_z}$, to the cross-sectional diameter. Curves for three different rod dielectric constants are shown: $\epsilon_r = 3.2$, $\epsilon_r = 2.6$, and $\epsilon_r = 2.2$. The DRA used in this work has $\epsilon_r = 2.6$. The lower and upper limits of the recommended value for $\frac{\lambda}{\lambda_z}$ at the feed of a surface wave antenna are marked.

The majority of published dielectric rod antennas are fed by metallic waveguides. Planar feeds have been demonstrated, but not explored in detail. Furthermore, there is no example known to the authors of a planar-fed DRA array. The background and theory laid out above are necessary to understanding the role the feed plays in the function and design of a single DRA and of the consequences of this design to that of an array. This understanding results in design procedures for planar-fed DRA arrays. With this foundation in place, future DRA arrays may be designed including the possibility for fully additive manufactured, moderate to high gain arrays.

III. Planar-Fed Dielectric Rod Antenna Design

The DRA design method presented here is based on empirical observations and involves a series of steps for optimizing the phase difference between the travelling wave outside the rod and inside the rod to shape the radiation pattern according to the discontinuity radiation concept. The total phase difference, ϕ, over the length of a generic constant diameter dielectric rod, l_{rod}, is shown in (1) in terms of the free space and surface wave propagation constants. This relationship is expressed in (2) in terms of the free space wavelength, λ, and the surface wave wavelength, λ_z. The diameter of a constant diameter rod is calculated from the associated wavelength ratio of (2) using Fig. 1.

$$k_z \cdot l_{rod} - k \cdot l_{rod} = \phi \tag{1}$$

$$\frac{\lambda}{\lambda_z} = 1 + \frac{\lambda \cdot \phi}{2 \cdot \pi \cdot l_{rod}} \tag{2}$$

A. Design for Maximum Gain

The maximum theoretical gain of DRAs is determined by analogy to Yagi-Uda antennas, which are another type of surface wave antenna. For Yagi-Uda antennas with total length between 3λ and 8λ as measured from the beginning of the feed to the terminal plane, the gain is calculated by (3) [29], [48]. This expression of gain is feed dependent. In simulations of planar-fed DRAs of varying length, we have found (3) to be the maximum gain associated with the length of the constant diameter section of Fig. 2. In this case, (3) corresponds to the maximum gain for a constant diameter DRA between 3λ and 8λ in length assuming high excitation efficiency at the feed end and a good match to free space at the terminal end. A taper is added to the feed end of the rod to maximize excitation efficiency and to ensure a fully formed surface wave at the beginning of the constant diameter rod. Another taper is added to the terminal end of the constant diameter rod to match the surface wave to free space by rapidly increasing the surface wave velocity to match the free space wave velocity.

$$Gain = \frac{10 \cdot l_{rod}}{\lambda} \tag{3}$$

Ehrenspeck and Poehler [48] examined the optimal phase difference along Yagi-Uda antennas for maximum gain. They determined, for antennas between 4λ and 8λ in length, a phase difference at the end of the antenna of approximately $120°$ is optimal for maximum gain. This phase difference is ϕ in (1). For the planar-fed DRAs examined here, it has been found

This article has been accepted for publication in a future issue of this journal, but has not been fully edited. Content may change prior to final publication. Citation information: DOI 10.1109/OJAP.2021.3081992, IEEE Open Journal of Antennas and Propagation

that the maximum gain of (3) is obtained when the 120° phase difference is approximately equally divided over l_{cd} and the feed taper. This finding is consistent with the minimum length required to ensure a fully formed surface wave by the end of the feed taper; the minimum length is one that will produce a 60° phase difference after a feed discontinuity [29]. There are two such discontinuities for the DRA designs studied here: the feed of the DRA corresponding to the beginning of the feed taper, and the end of the feed taper launching its surface wave onto the constant diameter section.

$$\frac{\lambda}{\lambda_z} = 1 + \frac{\lambda}{6 \cdot l_{cd}} \tag{4}$$

Our design procedure for a planar-fed DRA is a modified version of Zucker's design guidelines for surface wave antennas and is summarized as follows:

1) For a desired length of l_{cd}, the maximum gain is determined according to (3). Eq. (3) may also be used to determine the necessary value for l_{cd} to achieve a desired gain.
2) The diameter d_2 is calculated from the $\frac{\lambda}{\lambda_z}$ value from (4) using the desired value of l_{cd} and Fig. 1. This value of d_2 ensures a phase difference of 60° along l_{cd}.
3) For surface wave antennas the recommended value for $\frac{\lambda}{\lambda_z}$ at the feed is between 1.2 and 1.3. For a planar-fed DRA, the optimal value for d_1 at the feed found by optimization is the diameter associated with $\frac{\lambda}{\lambda_z} = 1.3$, as determined from Fig. 1. If the initial diameter of the rod is too large, the incident wave travels within the rod and there is no surface wave. If the diameter is too small, the rod doesn't interact with the incident wave from the feed. The resulting diameter at the feed is larger and the surface wave is slower than at any other point along the rod.
4) The feed taper length is selected to be approximately 25% of l_{cd}, following recommendations based on empirical work for Yagi-Uda antennas in [29]. Full-wave simulations for the designs herein confirm that this provides the optimal gain, and a step-wise approximation of the phase contributed by the taper from d_1 to d_2 shows approximately 70 degrees of phase shift along l_{ft}. This is close to the value of 60 degrees mentioned above.
5) For best match of the radiating end of the DRA to free space, the phase velocity of the surface wave should be the same as that of free space: $\frac{\lambda}{\lambda_z} = 1$. This is accomplished by choosing the value of d_3 associated with $\frac{\lambda}{\lambda_z} = 1$ from Fig. 1. The terminal taper length, l_{tt}, is 0.5λ long.

Fig. 2 illustrates a planar-fed DRA designed using the above method. The resulting dimensions of a 15 GHz DRA design using this design method are outlined in Table I. Table II summarizes the performance of the individual planar-fed DRA. The simulated DRA gain is within 0.3 dB of the theoretical gain. The simulations assume 100% infil ABS with $\epsilon_r = 2.6$ and tan $\delta = 0.0052$. The substrate is 0.5 mm thick Rogers 4003 substrate, $\epsilon_r = 3.55$ and tan $\delta = 0.0027$, with 17 um thick copper.

TABLE I: Summary of DRA dimensions (mm)

Constant Diameter Length: l_{cd}	96
Feed Taper Length: l_{ft}	24
Terminal Taper Length: l_{tt}	10
Feed to Terminal Taper: $l_{ft} + l_{cd}$	120
Feed Diameter: d_1	12.4
Constant Diameter: d_2	6.8
Terminal Diameter: d_3	4.2

TABLE II: Summary of DRA performance

Theoretical Gain (dBi), Eq. (3)	16.8
Simulated Gain (dBi)	16.5
Simulated 3dB Beamwidth (deg)	26
Simulated Sidelobe Level (dB)	-16

IV. Efficient Excitation and the Planar Feed

By the discontinuity radiation concept, radiation occurs at discontinuities along the rod. The feed is one such discontinuity. The objective of feed design is maximum power transfer into the surface wave. However, since the feed is a discontinuity, there will be radiation. As detailed above, the radiation from the feed contributes to the final radiation pattern of the DRA.

Not much has been written about using a planar circuit structure as a feed for DRAs or, alternatively, using DRAs to enhance the performance of planar radiators. However, planar feeds have been successfully demonstrated [18], [21]. The planar feed is similar to the hollow metallic waveguide feed in that both have a radiating aperture. The surface of the planar radiator and the plane corresponding to the open termination of the metallic waveguide both present mode configurations similar to the dominant surface wave mode. Placing a DRA directly on a planar radiator is therefore conceptually similar to placing a DRA at the radiating aperture of an open metallic waveguide, although there are important differences.

The fundamental TE_{10} and TE_{11} mode in the hollow metallic rectangular and circular waveguides, respectively, are similar to the HE_{11} hybrid dominant mode in the circular cross-section DRA. In the metallic waveguide-fed DRAs of Fig. 3, tapering the dielectric inside the metallic waveguide creates a gradual transition from the inside of the waveguide to the surface of the rod, which results in less reflection and

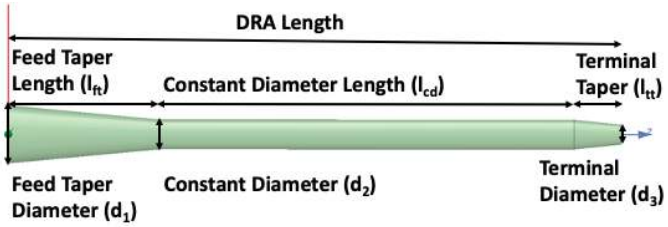

Fig. 2: Maximum gain design for circular cross-section planar-fed DRA.

This article has been accepted for publication in a future issue of this journal, but has not been fully edited. Content may change prior to final publication. Citation information: DOI 10.1109/OJAP.2021.3081992, IEEE Open Journal of Antennas and Propagation

more power available for both the surface wave and radiation from the feed.

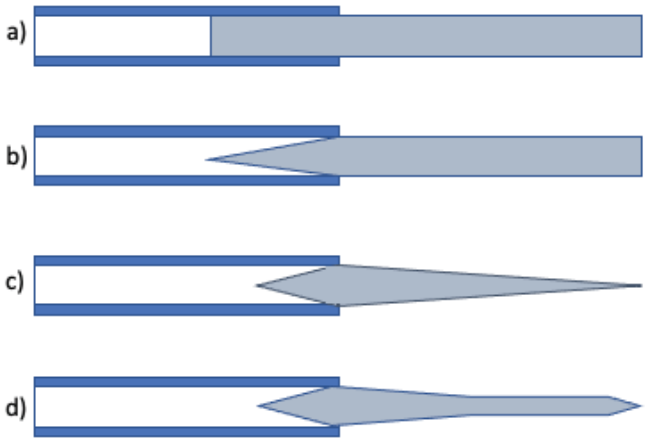

Fig. 3: Dielectric rod antennas with hollow waveguide feeds: a) Uniform DRA inserted into waveguide feed, b) uniform DRA with matching taper inserted into waveguide feed, c) continuous taper dielectric rod with matching taper inserted into waveguide, d) maximum gain DRA design according to [29]

The matching taper is not possible for planar DRA feeds. Matching the planar radiator feed to the DRA is accomplished by modelling the planar radiator as a conductor layer on a thin, high dielectric substrate backed by an infinite dielectric block of the same material as the DRA. Failure to include the infinite dielectric backing will result in a shift in the resonant frequency of the slot antenna when in contact with the DRA.

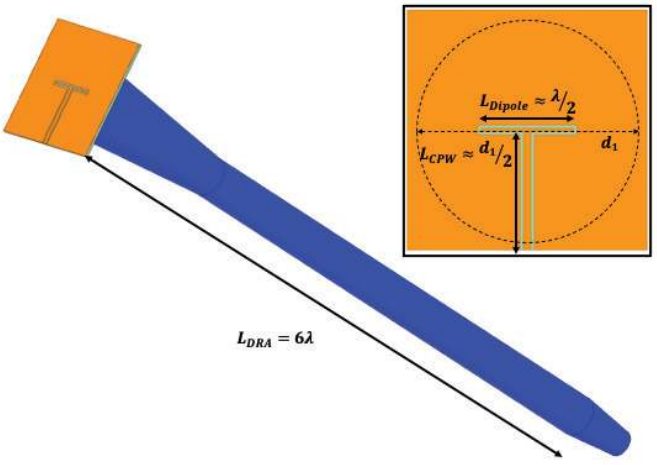

Fig. 4: Folded dipole slot-fed DRA. The folded dipole slot antenna is fed by coplanar waveguide (CPW) (inset). The dotted circle illustrates the footprint of the DRA under the dipole-slot feed.

A folded dipole slot antenna is used here as the planar feed for each DRA in the 2 x 2 array. The DRA acts as a thick dielectric backing to the dipole slot substrate. The design of the folded dipole slot antenna, as with other patch and slot antennas, necessarily takes the material characteristics and thickness of the dielectric substrate into account. The radiator is designed for the effective dielectric constant of its substrate backed by an infinite slab of the DRA material.

A CPW is used to feed the folded dipole slot in order to present a balanced feed to the slot. The impedance of the folded dipole slot is high enough to be more easily matched to the planar array feed with a $50\ \Omega$ input impedance. Simmons [49] gives detailed design procedures for CPW backed by an infinite dielectric substrate.

The thin substrate layer is 0.5 mm thick Rogers 4003C. The CPW feed is 6 mm long with a 0.254 mm gap width. The folded dipole slot is 7.72 mm long and 0.76 mm wide. The center spacing between the slots of the folded dipole is 0.252 mm wide. The feed dimensions of the rod are summarized in Table IV.

The simulated fields associated with the planar-fed DRA are shown in Figs. 5 and 6. Figs. 5a and 6a show the fields associated with the planar feed without the DRA from two different points of view. In these figures, the dipole pattern is clearly seen, radiating evenly in both directions away from the radiator. The effect of adding the DRA to the planar feed is seen in the field plots of Figs. 5b and 6b. In each case, the field tends toward the DRA, radiating predominately along the DRA axis. The beginning of the formation of a surface wave is most clearly seen at the boundary of the DRA in Fig. 6b.

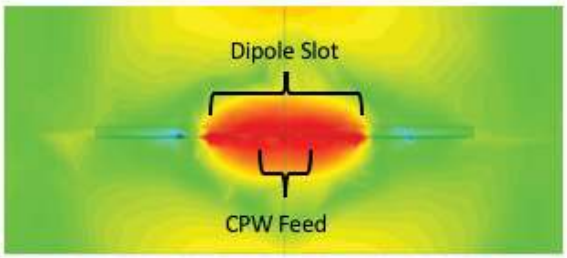

(a) E-field without DRA

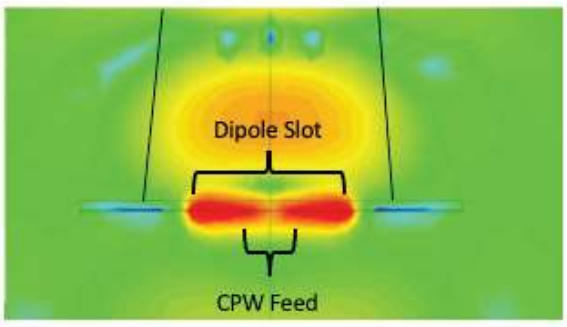

(b) E-field with DRA

Fig. 5: Comparison of the electric field in the CPW feed and folded dipole slot with and without the DRA as seen from the CPW feed looking toward the DRA. The dipole pattern is visible in the a). The wave inside the DRA is visible in b).

V. Simulated Performance of the Planar-fed DRA

Fig. 7 compares the S_{11} of the folded dipole slot-fed DRA and a folded dipole slot backed by a half-spaced filled with

This article has been accepted for publication in a future issue of this journal, but has not been fully edited. Content may change prior to final publication. Citation information: DOI 10.1109/OJAP.2021.3081992, IEEE Open Journal of Antennas and Propagation

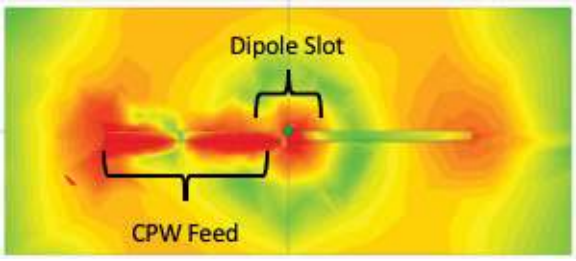

(a) E-field without DRA

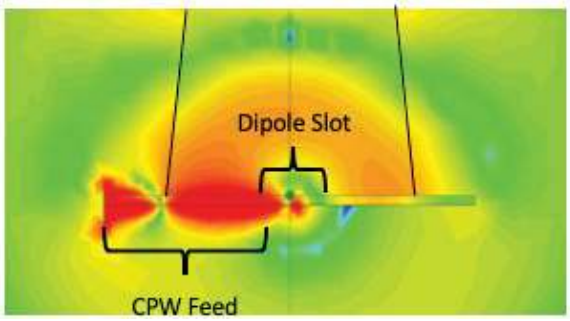

(b) E-field with DRA

Fig. 6: Comparison of the electric field in the CPW feed and folded dipole slot with and without the DRA viewed normal to the CPW feed, along the folded dipole slot. The dipole pattern is seen in a). The beginning of the formation of the surface wave is seen in b).

the same material as the DRA. The S_{11} of the planar-fed DRA is that of a resonant planar dipole slot antenna. It has a single, deep resonance and the bandwidth of a dipole slot. This is as expected since the design is fundamentally that of a dipole slot taking into account its unique substrate: that of the DRA.

Fig. 8 compares the simulated radiation efficiency of the DRA with a lossless substrate and conductor layer to the simulated radiation efficiency of the DRA with a lossy substrate and conductor layer. Losses in the feed have minimal impact on the radiation efficiency across the band. The radiation efficiency of the planar feed is greater than 90% from 12 GHz to 18 GHz. Losses in the substrate and conductor account for about 5% reduction in the radiation efficiency across the band. The reference plane for the single DRA simulations is shown in Fig. 10. Even though DRAs are typically fed with hollow metallic waveguides, this shows the viability of planar-integrated DRAs without them. Table III compares existing planar-fed designs both with and without hollow metallic waveguides. The performance is similar in all cases.

VI. Planar-fed Dielectric Rod Antenna Array

A. DRA Array Design

For an array of DRAs with limited mutual impedance, the maximum theoretical gain is that of a surface wave antenna array. The spacing between the elements influences the gain of the array. In order to approach this maximum theoretical gain, the spacing between the centers of the individual elements, d_s, is chosen according to the approximation of (5) [29], where l is the DRA length and λ is the free space wavelength. The

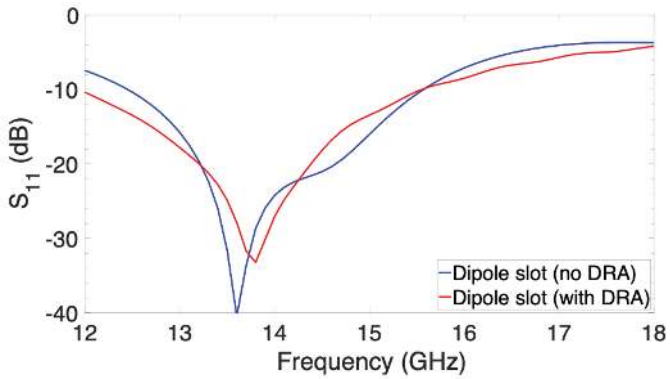

Fig. 7: Simulated S_{11} of a planar folded dipole slot-fed DRA as compared to the same feed without the DRA. For the feed without the DRA, the substrate of the folded dipole slot is backed by an infinite block of the same material as the DRA.

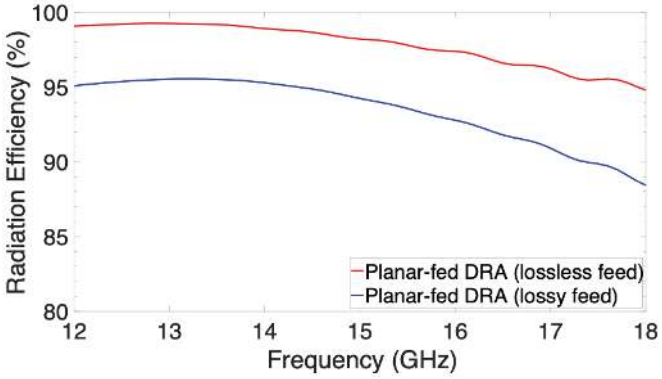

Fig. 8: Comparison of simulated DRA radiation efficiencies of the planar-fed DRA with a lossy substrate and conductor and the same DRA with a lossless substrate and conductor. The DRA material is lossy in both cases.

TABLE III: Planar-integrated DRAs

Type	**S_{11} (dB)**	**Reported/ Theoretical Gain (dBi)**	**DRA Length (λ_0)**
Slot with waveguide [19]	-18	11 / 12	1.4
Microstrip coupled slot with waveguide [20]	-14	18 / 21	13
Ring slot-fed [26]	Not reported	12 / 13	2
Patch with waveguide [50]	-15	16 / 18	6
Dipole slot-fed (Section III)	-19	16 / 18	6

lower limit of (5) is a minimum spacing guideline to maintain mutual coupling between elements of at most $-10\ dB$. The upper spacing limit of (5) maximizes attenuation in the first principle sidelobe. Pattern multiplication of the individual element pattern and the underlying array factor results in an increase in the array pattern gain on boresight as shown in Fig. 9. The main lobe of the elements is narrowed by the deep nulls in the array factor nearer to boresight than in the element pattern.

$$0.5\sqrt{\frac{l}{\lambda}} \leq \frac{d_s}{\lambda} \leq \sqrt{\frac{l}{\lambda}} \tag{5}$$

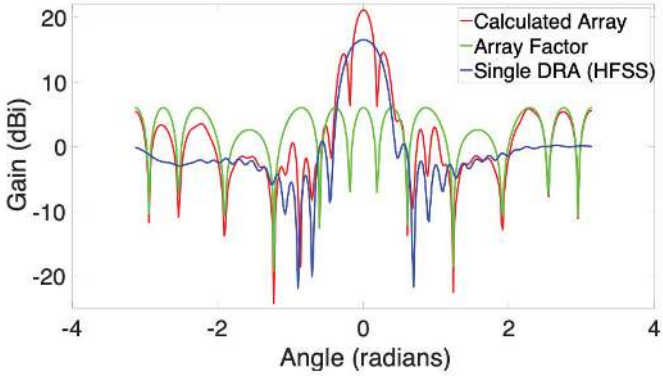

Fig. 9: Calculated radiation pattern for the 2 x 2 DRA array. The array factor is multiplied with the simulated individual element pattern to produce the theoretical array radiation pattern.

Following these element spacing guidelines, the spacing for 6λ long planar-fed DRAs at 15 GHz should be between 24.5 mm and 49.0 mm. Optimizing the gain in simulation resulted in 52 mm spacing for maximum gain in the array. This is a slightly larger spacing than what is estimated by (5).

The folded dipole slot is fed by the CPW feed of length L_{CPW} (Fig. 10). The three line coupler represented by the W1, W2, and W3 in Fig. 10 transitions the grounded microstrip feed into the ungrounded CPW dipole slot feed. The microstrip to coplanar waveguide transition is as described in [49]. Ungrounded CPW is chosen to allow the radiation from the dipole slot antenna to travel to the dielectric rod without interference from a nearby ground plane. This transition section at each of the four dipole slots makes the corporate, grounded microstrip array feed of Fig. 11 possible.

The rest of the array feed is a grounded microstrip corporate feed as in Figs. 11 and 12. The ground layer only runs beneath the microstrip feed and the individual three-line coupler transition sections and is annotated in Fig. 12. The dimensions of the planar array feed are listed in Table IV.

The array of folded dipole slots are excited simultaneously, in phase, from a single $50\ \Omega$ input. The $50\ \Omega$ array input impedance is transformed to $25\ \Omega$ by a quarter-wave impedance transformer before the first $3\ dB$ power divider, resulting in two $50\ \Omega$ microstrip lines. These two $50\ \Omega$ microstrip lines are divided again by two respective $3\ dB$ power dividers, resulting in a phase-aligned $100\ \Omega$ input to each of the four folded dipole slots.

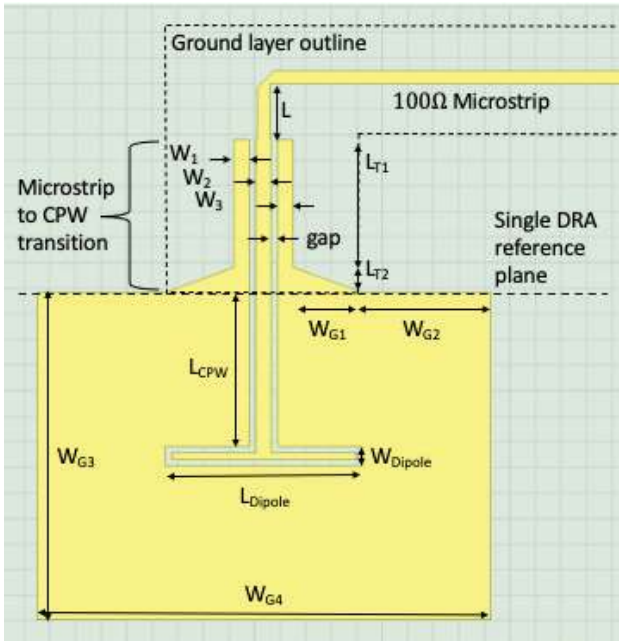

Fig. 10: Single antenna array element. Folded dipole slot fed by a $100\ \Omega$ microstrip line. The microstrip to CPW transition converts the fields in the grounded microstrip line into the ungrounded CPW feed, which is a balanced feed for the folded dipole slot antenna. The ground layer of Fig. 12 is represented by the dotted outline. The reference plane of the single DRA of Section III is marked.

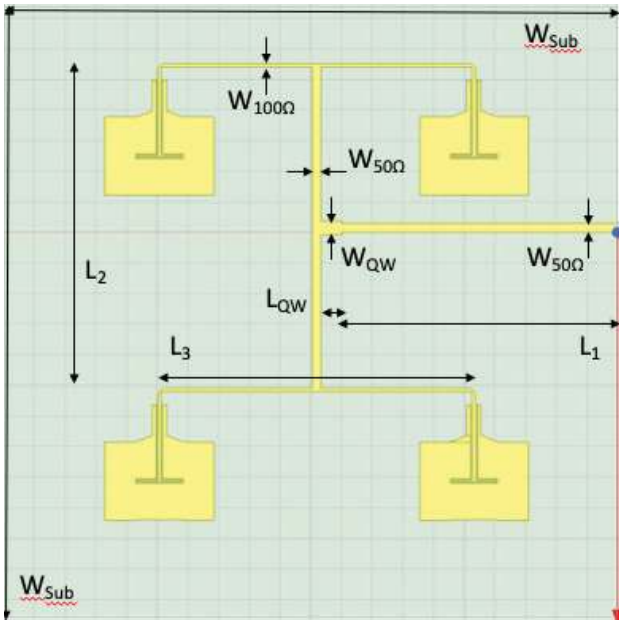

Fig. 11: The four-element folded dipole slot array and feed network. The $50\ \Omega$ input impedance feeds four individual $100\ \Omega$ inputs using a quarter wave transformer and three $3\ dB$ power dividers.

This article has been accepted for publication in a future issue of this journal, but has not been fully edited. Content may change prior to final publication. Citation information: DOI 10.1109/OJAP.2021.3081992, IEEE Open Journal of Antennas and Propagation

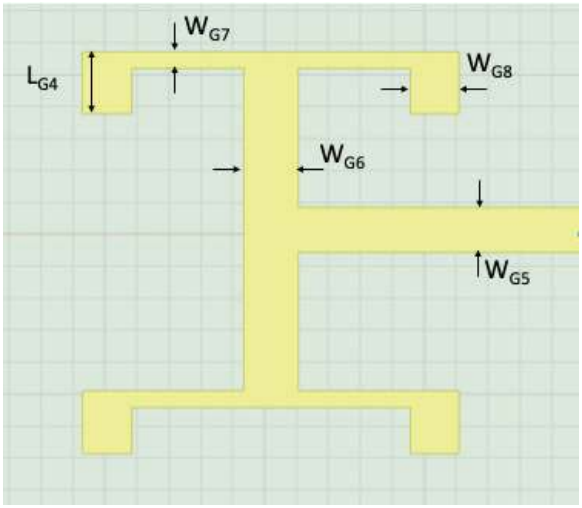

Fig. 12: Array ground trace. This layer is on the opposite side of the substrate from Fig. 11.

TABLE IV: Summary of array feed dimensions (mm)

L	2.19	$\mathbf{L}_{T1}$	5	$\mathbf{L}_{T2}$	1
$\mathbf{W}_1$	0.6	$\mathbf{W}_2$	0.6	$\mathbf{W}_3$	0.6
gap	0.254	$\mathbf{W}_{G1}$	2.7	$\mathbf{W}_{G2}$	5
$\mathbf{W}_{G3}$	12.79	$\mathbf{W}_{G4}$	17.72	$\mathbf{L}_{CPW}$	6
$\mathbf{W}_{Dipole}$	0.76	$\mathbf{L}_{Dipole}$	7.72	$\mathbf{W}_Sub$	100
$\mathbf{L}_1$	45	$\mathbf{L}_2$	52.55	$\mathbf{L}_3$	50.77
$\mathbf{W}_{QW}$	3.3	$\mathbf{L}_{QW}$	2.28	$\mathbf{W}_{50\ \Omega}$	1.39
$\mathbf{W}_{100\ \Omega}$	0.5	$\mathbf{L}_{G4}$	9.69	$\mathbf{W}_{G5}$	6.95
$\mathbf{W}_{G6}$	8.5	$\mathbf{W}_{G7}$	2.5	$\mathbf{W}_{G8}$	7.72

B. Fabrication

The planar antenna and array feed are built on 0.508 mm thick Rogers 4003C material with a dielectric constant $\epsilon_r = 3.55$. The solid, circular cross-section dielectric rods are 3D printed using the fused deposition modelling technique with 100% infil ABS plastic with $\epsilon_r = 2.6$ and a 0.0052 dielectric loss tangent.

The diameter d_2 of the fabricated rod used in the array design is 6.68mm, which is slightly smaller than the value listed in Table I. This minor difference did not significantly change the simulated performance of the individual DRA.

Each rod is 6λ long at 15 GHz, 120 mm, plus the added length of the Terminal Taper of Fig. 2, 10 mm, for a total length of 130 mm. At 130 mm length, these rods were approaching the z-axis height limit of many 3D printers. Without a sturdy printed base, the rods begin to physically oscillate, destroying the consistency of the print toward the end of the rod. Longer 3D printed rods, though desirable for higher gain, may not be easily printed with desktop 3D printers.

The Rogers 4003C was milled using standard PCB milling techniques. The DRAs were 3D printed vertically from the feed on the printer plate upward to the end of the terminal taper. The individual DRAs were glued to the substrate side of each dipole slot by hand. The final array is shown in a near field range at NSI-MI in Suwanee, GA in Fig. 13.

C. Performance: Simulation vs Measurement

The individual element gain simulated in HFSS is $16.5\ dBi$. According to (6), the theoretical array gain for this 4 element array is $22\ dBi$. When calculated from array theory by pattern multiplication of the simulated individual element pattern with the array factor, the gain is $21\ dBi$.

$$ArrayGain = n \cdot Gain_{Element} = n \cdot \frac{10 \cdot l_{cd}}{\lambda} \qquad (6)$$

Antenna measurements were taken at NSI-MI and the Georgia Institute of Technology. The simulated and measured S_{11} are compared in Fig. 14. The measured S_{11} shows good agreement to simulation. The simulated, calculated, and measured array patterns are compared in Fig. 15. The calculated pattern accounts for losses in the array feed and the radiation efficiency. Its peak gain is almost 3 dB lower than the expected array gain at 15 GHz. The simulated and measured patterns show good agreement. The measured gain is $19\ dBi$, which is $0.3\ dB$ below the simulated gain of $19.3\ dBi$. Both simulated and measured patterns have a $3\ dB$ beamwidth of 8 degrees with the first sidelobes $10\ dB$ below the gain of the main lobe. The $3\ dB$ gain bandwidth of the array is 26% (Fig. 16) and the radiation efficiency of the array at 15 GHz is 80%, as in Fig. 17. The simulated and measured gain vs frequency plots of Figure 16 demonstrate some limited differences, especially at higher frequencies. Two sources of loss exist in this work which have not been captured in simulation: minor variations in spacing and alignment resulting from manual integration of the DRAs to the planar feed and surface roughness along the milled lines of the feed network.

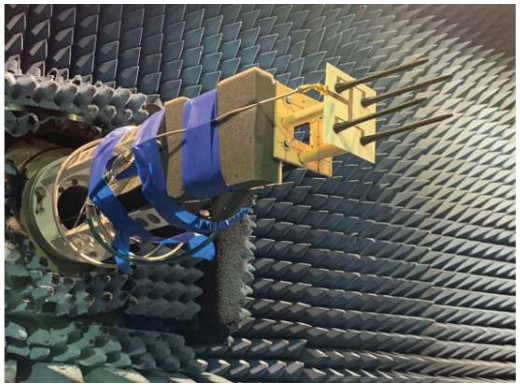

Fig. 13: Array test setup at NSI-MI, Suwanee, GA

VII. Conclusions

A fabricated 2 x 2 array of folded dipole slot antenna fed DRAs achieves a gain $19\ dBi$ with a $3\ dB$ gain bandwidth of 26%. The 4-element array is simple, cost-effective to fabricate, being made with standard PCB processes and 3D printed ABS plastic DRAs, and may be scaled into the mm-wave regime. Future iterations of this design may take advantage of earlier work in cladded dielectric rod antennas [7] to further customize the size, footprint, weight, and robustness of the

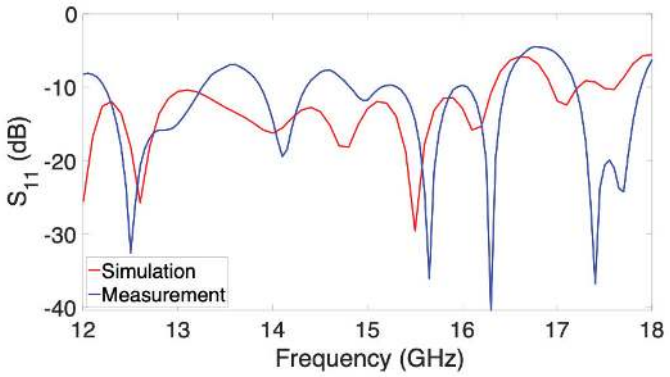

Fig. 14: Simulated array S_{11} compared to measured array S_{11}.

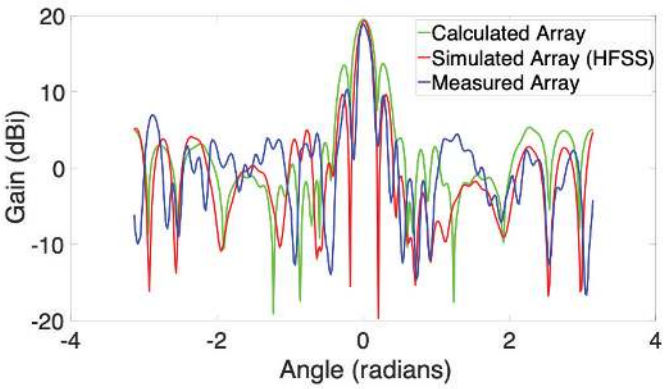

Fig. 15: Comparison of the calculated, simulated, and measured DRA array radiation patterns at 15 GHz.

array by printing high dielectric constant rods embedded in lower dielectric, 3D printed cladding.

ACKNOWLEDGMENT

The authors would like to thank NSI-MI in Suwanee, GA and the Georgia Institute of Technology for their help with access to measurement equipment and facilities during the COVID-19 pandemic. This work would not have been possible otherwise.

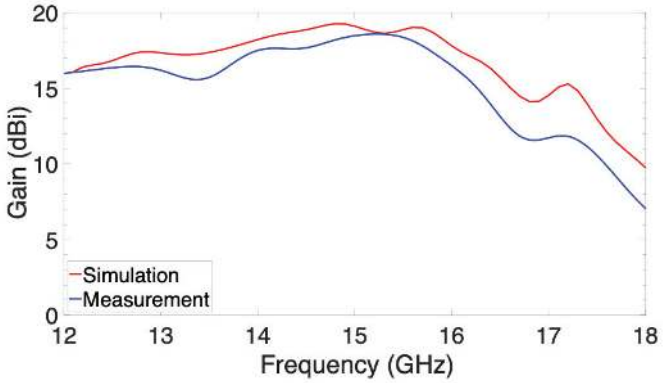

Fig. 16: Comparison of simulated and measured array gain versus frequency.

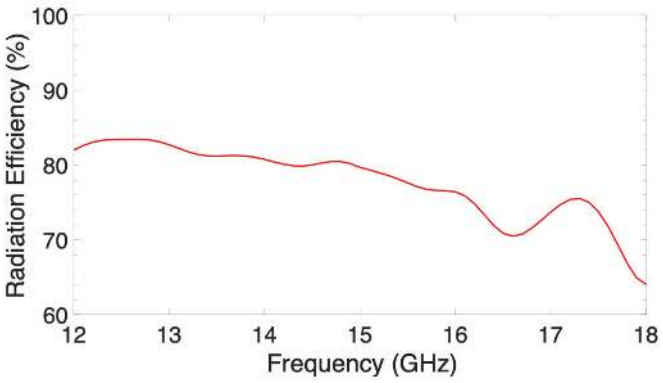

Fig. 17: Simulated (HFSS) array radiation efficiency.

REFERENCES

[1] S. P. Skobelev, *Phased Array Antennas with Optimized Element Patterns*. Norwood, MA: Artech House, 2011.

[2] G. E. Mueller and W. A. Tyrrell, "Polyrod Antennas," *Bell System Technical Journal*, vol. 26, no. 4, pp. 837–851, 1947.

[3] C. Kumar, V. S. Kumar, and V. V. Srinivasan, "Design aspects of a compact dual band feed using dielectric rod antennas with multiple element monopulse tracking," *IEEE Transactions on Antennas and Propagation*, vol. 61, no. 10, pp. 4926–4932, 2013.

[4] J.-h. Qiu and N.-n. Wang, "Optimized Dielectric Rod Antenna for Millimeter Wave FPA Imaging System," *Imaging Systems and Techniques*, pp. 147–150, 2009.

[5] R. Kazemi, A. E. Fathy, and R. A. Sadeghzadeh, "Dielectric rod antenna array with substrate integrated waveguide planar feed network for wideband applications," *IEEE Transactions on Antennas and Propagation*, vol. 60, no. 3, pp. 1312–1319, 2012.

[6] M. W. Rousstia and M. H. Herben, "60-GHz wideband branchline coupler and patch antenna with dielectric rod for full-duplex gigabit wireless communication," *8th European Conference on Antennas and Propagation, EuCAP 2014*, no. EuCAP, pp. 201–205, 2014.

[7] G. L. Saffold and T. M. Weller, "Design of Cladded Dielectric Rod Antennas," in *2019 IEEE 20th Wireless and Microwave Technology Conference, WAMICON 2019*, 2019.

[8] D. C. Lugo, R. A. Ramirez, J. Wang, and T. M. Weller, "Ku band Metal-Strip-Loaded Dielectric Rod Antenna with Narrowband Gain Enhancement," *IEEE International Symposium on Antennas and Propagation & USNC/URSI National Radio Science Meeting*, pp. 1889–1890, 2018.

[9] J. Richter and L. P. Schmidt, "Dielectric rod antennas as optimized feed elements for focal plane arrays," *IEEE Antennas and Propagation Society, AP-S International Symposium (Digest)*, vol. 3 A, pp. 667–670, 2005.

[10] a. a. Generalov, D. V. Lioubtchenko, and a. V. Räisänen, "Dielectric rod waveguide antenna for 220-325 GHz," *Proceedings of 6th European Conference on Antennas and Propagation, EuCAP 2012*, pp. 3551–3553, 2012.

[11] S. Kobayashi, R. Lampe, N. Deo, and R. Mittra, "Dielectric Antennas for Millimeter-Wave Applications," University of Illinois, Urbana, Tech. Rep., 1980.

[12] S. Kobayashi, R. Mittra, and R. Lampe, "Dielectric tapered rod antennas for millimeter-wave applications," *IEEE Transactions on Antennas and Propagation*, vol. 30, no. 1, pp. 54–58, 1982. [Online]. Available: http://ieeexplore.ieee.org/lpdocs/epic03/wrapper.htm?arnumber=1142758

[13] T. Ando, J. Yamauchi, and H. Nakano, "Rectangular dielectric-rod fed by metallic waveguide," *IEE Proceedings - Microwaves, Antennas and Propagation*, vol. 149, no. 2, p. 92, 2002.

[14] L. Mickey and G. Chadwick, "Closely Spaced High Dielectric Constant Polyrod Arrays," *IRE International Convention Record*, vol. 1, p. 213, 1958.

[15] D. C. Lugo, R. A. Ramirez, J. Castro, J. Wang, and T. M. Weller, "3D printed multilayer mm-wave dielectric rod antenna with enhanced gain," *2017 IEEE Antennas and Propagation Society International Symposium, Proceedings*, vol. 2017-Janua, pp. 1247–1248, 2017.

[16] J. P. Pousi, D. V. Lioubtchenko, S. N. Dudorov, J. A. Mallat, and A. V. Räisänen, "High permittivity dielectric ROD waveguide antenna for 110-

150 GHz," *European Space Agency, (Special Publication) ESA SP*, vol. 626 SP, 2006.

[17] J. Pousi, D. Lioubtchenko, S. Dudorov, and A. Raisanen, "High permittivity dielectric rod waveguide as an antenna array element for millimeter waves," *IEEE Transactions on Antennas and Propagation*, vol. 58, no. 3, pp. 714–719, 2010. [Online]. Available: http://ieeexplore.ieee.org/xpls/abs{_}all.jsp?arnumber=5361326

[18] Y. Liu, X. Chen, G. Xu, C. Liu, and K. Huang, "A high gain and simple-structured dielectric resonator antenna array with cylindrical rods and microstrip feeding," *International Journal of Applied Electromagnetics and Mechanics*, vol. 47, pp. 433–440, 2015.

[19] Z. Ahmad and J. Hesselbarth, "Millimeterwave dielectric rod antenna with a circuit board surface mount feed," *GeMiC 2018 - 2018 German Microwave Conference*, vol. 2018-Janua, pp. 145–147, 2018.

[20] F. Poprawa, A. Zanati, A. Ziroft, and F. Ellinger, "Waveguide transition to feed a fully PCB integrated dielectric rod antenna," *IEEE MTT-S International Microwave Symposium Digest*, vol. 2, pp. 640–643, 2010.

[21] K. C. Huang and Z. Wang, "V-Band Patch-Fed Rod Antennas for High Data-Rate Wireless Communications," *IEEE Transactions on Antennas and Propagation*, vol. 54, no. 1, pp. 297–300, 2006.

[22] T.-S. Chu and N. Kilcoyne, "The Excitation of a Dielectric-Rod Antenna by a Helix," *IEEE Transactions on Antennas and Propagation*, vol. 9, no. 4, p. 2, 1961.

[23] A. J. Abumunshar and K. Sertel, "5:1 Bandwidth Dielectric Rod Antenna Using a Novel Feed Structure," *IEEE Transactions on Antennas and Propagation*, vol. 65, no. 5, pp. 2208–2214, 2017.

[24] C. W. Liu and C. C. Chen, "A UWB three-layer dielectric rod antenna with constant gain, pattern and phase center," *IEEE Transactions on Antennas and Propagation*, vol. 60, no. 10, pp. 4500–4508, 2012.

[25] H. Zhou, X. Chen, D. S. Espinoza, A. Mickelson, and D. S. Filipovic, "Nanoscale optical dielectric rod antenna for on-chip interconnecting networks," *IEEE Transactions on Microwave Theory and Techniques*, vol. 59, no. 10 PART 2, pp. 2624–2632, 2011.

[26] S. M. Hanham, T. S. Bird, A. D. Hellicar, and R. A. Minasian, "Evolved-profile dielectric rod antennas," *IEEE Transactions on Antennas and Propagation*, vol. 59, no. 4, pp. 1113–1122, 2011.

[27] A. Rivera-Lavado, L. E. García-Muñoz, D. Lioubtchenko, S. Preu, D. Segovia-Vargas, and A. V. Räisänen, "Increasing the bandwidth of dielectric rod waveguide antennas for terahertz applications," in *2015 40th International Conference on Infrared, Millimeter, and Terahertz waves (IRMMW-THz)*, 2015, pp. 1–1.

[28] A. Rivera-Lavado, S. Preu, L. E. Garcia-Munoz, A. Generalov, J. Montero-de Paz, G. Dohler, D. Lioubtchenko, M. Mendez-Aller, F. Sedlmeir, M. Schneidereit, H. G. L. Schwefel, S. Malzer, D. Segovia-Vargas, and A. V. Raisanen, "Dielectric Rod Waveguide Antenna as THz Emitter for Photomixing Devices," *Antennas and Propagation, IEEE Transactions on*, vol. 63, no. 3, pp. 882–890, 2015.

[29] F. J. Zucker, "Surface Wave Antennas," in *Antenna Engineering Handbook, Fourth Edition*, 2007, pp. 10–1 – 10–32. [Online]. Available: http://mhebooklibrary.com/doi/book/10.1036/0071475745

[30] D. G. Kiely, *Dielectric Aerials*. Methuen and Company, 1953.

[31] D. Hondros and P. Debye, "Elektromagnetische Wellen an dielektrischen Drähten," *Annalen der Physik*, vol. 337, no. 8, pp. 465–476, 1910.

[32] D. Halliday and D. G. Kiely, "Dielectric Rod Aerials," *Journal of the Institution of Electrical Engineers - Part IIIA: Radiocommunication*, vol. 94, pp. 610–618, 1947.

[33] G. Wilkes, "Wavelength Lenses," *Proceedings of the IRE*, vol. 36, no. 2, pp. 206–212, 1948.

[34] R. B. Watson and C. W. Horton, "The radiation patterns of dielectric rods - Experiment and theory," *Journal of Applied Physics*, vol. 19, no. 7, pp. 661–670, 1948.

[35] M. Bouix, "Contribution a l'étude des antennes diélectriques," *Annales des Télécommunications*, vol. 7, no. 6, pp. 276–295, 1952.

[36] A. FRADIN, "Dielectric Antennas," *Microwave Antennas*, pp. 511–584, 1961.

[37] J. Brown and J. O. Spector, "The radiating properties of end-fire aerials," *Proc. IEE*, no. 2216, pp. 27–34, 1957.

[38] J. James, "Theoretical investigation of cylindrical dielectric-rod antennas," *Proceedings of the Institution of Electrical Engineers*, vol. 114, no. 3, pp. 309–319, 1967.

[39] T. Ando, J. Yamauchi, and H. Nakano, "Numerical analysis of a dielectric rod antenna - Demonstration of the discontinuity-radiation concept," *IEEE Transactions on Antennas and Propagation*, vol. 51, no. 8, pp. 2007–2013, 2003.

[40] R. B. Watson and C. W. Horton, "On the calculation of radiation patterns of dielectric rods," *Journal of Applied Physics*, vol. 19, no. 9, pp. 836–837, 1948.

[41] C. W. Horton, F. C. Karal, and C. M. McKinney, "On the radiation patterns of dielectric rods of circular cross section - The TM01 mode," *Journal of Applied Physics*, vol. 21, no. 12, pp. 1279–1283, 1950.

[42] C. H. Chandler, "An investigation of dielectric rod as wave guide," *Journal of Applied Physics*, vol. 20, no. 12, pp. 1188–1192, 1949.

[43] W. M. Elsasser, "Attenuation in a dielectric circular rod," *Journal of Applied Physics*, vol. 20, no. 12, pp. 1193–1196, 1949.

[44] B. Thomas, "The Precise Mechanism of Radiation from Surface Wave Aerials," *The Journal of the Institution of Engineers, Australia*, vol. 9, no. 36, pp. 225–238, 1964.

[45] J. Simon and G. Weill, "Un Nouveau Type D'Aerien A Rayonnement Longitudinal," *Annales De Radioelectricite*, vol. July, no. 33, pp. 183–198, 1953.

[46] M. M. Astrahan, "Guided Waves on Hollow Dielectric Tubes," Dissertation, Northwestern University, 1949.

[47] W. C. J. Jakes, "Attenuation and Radiation Characteristics of Dielectric Tube Waveguides," Dissertation, Northwestern University, 1949.

[48] H. Ehrenspeck and H. Poehler, "A new method for obtaining maximum gain from yagi antennas," *IRE Transactions on Antennas and Propagation*, vol. 7, no. 4, pp. 379–386, oct 1959. [Online]. Available: http://ieeexplore.ieee.org/document/1144708/

[49] R. N. Simons, *Conventional Coplanar Waveguide*. John Wiley and Sons, 2003, vol. 7.

[50] K. C. Huang and Z. Wang, "Millimeter-Wave Circular Polarized Beam-Steering Antenna Array for Gigabit Wireless Communications," *IEEE Transactions on Antennas and Propagation*, vol. 54, no. 2, pp. 743–746, 2006.

Gabriel L. Saffold (M'04) received the B.S. degree in electrical engineering from the University of South Florida in Tampa, FL in 2005 and the M.S. degree in electrical engineering from the University of New Mexico in Albuquerque, NM in 2017. He holds an A.A. in Liberal Arts, a B.A. in Biblical Studies from Florida College in Temple Terrace, FL, a Masters in Strategic Intelligence/Intelligence Operations from American Military University, and a M.S. in Entrepreneurship in Applied Technologies from the University of South Florida. He is currently pursuing his PhD in electrical engineering at the University of South Florida.

Thomas M. Weller joined Oregon State University in 2018, as professor and head of the School of Electrical Engineering and Computer Science. He was a faculty member at the University of South Florida from 1995-2018, and received a PhD in Electrical Engineering from the University of Michigan in 1995. Weller's research focuses on microwave circuits and antennas, including an emphasis on the use of additive manufacturing. He has published over 300 journal and conference papers and 3 book chapters, and holds 40 U.S. patents, and is a fellow of IEEE and the National Academy of Inventors.